J|A|C|S
ARTICLES
Published on Web 03/10/2006

Interplay of Stereoelectronic and Enviromental Effects in Tuning the Structural and Magnetic Properties of a Prototypical Spin Probe: Further Insights from a First Principle Dynamical Approach

Michele Pavone,[†] Paola Cimino,[‡] Filippo De Angelis,[§] and Vincenzo Barone*[,†]

Contribution from the Dipartimento di Chimica, Università di Napoli "FedericoII", Complesso Universitario di Monte Sant'Angelo Via Cintia, I-80126 Napoli, Italy, Dipartimento di Scienze Farmaceutiche, Università di Salerno, via Ponte don Melillo, 84084 Fisciano (SA), Italy, and Istituto CNR di Scienze e Tecnologie Molecolari (ISTM-CNR), c/o Dipartimento di Chimica, Università di Perugia, Via Elce di Sotto 8, I-60123 Perugia, Italy

Received November 2, 2005; E-mail: baronev@unina.it.

Abstract: The nitrogen isotropic hyperfine coupling constant (*hcc*) and the **g** tensor of a prototypical spin probe (di-*tert*-butyl nitroxide, DTBN) in aqueous solution have been investigated by means of an integrated computational approach including Car−Parrinello molecular dynamics and quantum mechanical calculations involving a discrete-continuum embedding. The quantitative agreement between computed and experimental parameters fully validates our integrated approach. Decoupling of the structural, dynamical, and environmental contributions acting onto the spectral observables allows an unbiased judgment of the role played by different effects in determining the overall experimental observables and highlights the importance of finite-temperature vibrational averaging. Together with their intrinsic interest, our results pave the route toward more reliable interpretations of EPR parameters of complex systems of biological and technological relevance.

I. Introduction

Aminoxyls (nitroxides) are characterized by a long-living spin-unpaired electronic ground state[1] and by molecular properties strongly dependent on the chemical environment embedding the NO moiety.[2] These features led to such a widespread application of nitroxide derivatives as spin labels,[3] spin probes,[4] redox probes,[5] or contrast agents[6] that it is quite difficult to overemphasize the relevance of this class of compounds in many fields of modern chemistry.[7] Historically, the dependence of magnetic and UV parameters on the environment has been interpreted in terms of a selective stabilization of one of the two resonance structures depicted by Scheme 1.

Scheme 1

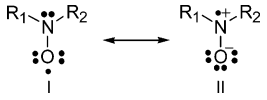

In particular, the solvent medium strongly affects the nitrogen *hcc (*hereafter A_N), which increases its value going from low to high dielectric constant medium, as it was experimentally reported by Knauer and Napier.[8] Unfortunately, no linear dependence or predictive formula has been found from the experiments in many different solutions. Several problems arise when considering protic solvents; whereas in aprotic solvents the dielectric contribution is the feature that mostly affects the molecular properties, the solute−solvent hydrogen bonding plays a key role which cannot be neglected or approximated within a dielectric-dependent theory. Moreover, the problems connected with this interpretation are emphasized when the nitroxide molecule is supposed to be at the interface between physically or chemically inhomogeneous systems, as they are commonly employed in experiments.[9] This issue has been recently high-

[†] Università di Napoli Federico II.
[‡] Università di Salerno.
[§] ISTM-CNR, Perugia.

(1) Keana, J. F. W. *Chem. Rev.* **1978**, *78*, 37.
(2) Improta, R.; Barone, V. *Chem. Rev.* **2004**, *104*, 1231.
(3) (a) Berliner, L. J., Ed. *Spin Labelling, Theory and Applications*; Academic Press: New York, 1976. (b) Stone, T. J.; Buckman, T.; Nordio, P. L.; McConnel, H.; *Proc. Natl. Acad. Sci. U.S.A.* **1965**, *54*, 1010.
(4) (a) Berliner, L. J. Ed. *Biological Magnetic Resonance, Spin Labeling in the Next Millennium*; Plenum Press: New York, 1998; Vol. 14. (b) Engström, M.; Vaara, J.; Schimelpfennig, B.; Ågren, H. J. *J. Phys. Chem. B* **2002**, *106*, 12354.
(5) (a) Baur, J. E.; Wang, S.; Brandt, M. C. *Anal. Chem.* **1996**, *68*, 3815. (b) Krzyczmonik, P. H. S. *J. Electroanal. Chem*. **1992**, *335*, 233.
(6) Brash, R. C.; London, D. A.; Wesbey, G. E.; Tozer, T. N.; Nirecki, D. E.; Williams, R. D.; Doemeny, J.; Tuck, L. d.; Lallemand, D. P. *Radiology* **1983**, *147*, 773.
(7) (a) Hayes Griffith, O.; Waggoner, A. S. *Acc. Chem. Res.* **1969**, *2*, 17. (b) Dugas, H. *Acc. Chem. Res.* **1977**, *10*, 47. (c) Hanson, P.; Millhauser, G.; Formaggio, F.; Crisma, M.; Toniolo, C. *J. Am. Chem. Soc.* **1996**, *118*, 7618. (d) Miller, T. R.; Alley, S. C.; Reese, A. W.; Solomon, M. S.; McCallister, W. V.; Mailer, C.; Robinson, B. H.; Hopkins, P. B. *J. Am. Chem. Soc.* **1995**, *117*, 9377. (e) Pyter, R. A.; Ramachandran, C.; Mukerjee, P. *J. Phys. Chem.* **1982**, *86*, 3206. (f) Greenspoon, N.; Wachet, E. *J. Am. Chem. Soc.* **1991**, *113*, 7233. (g) Ionita, P.; Caragheorgheopol, A. *J. Am. Chem. Soc.* **2002**, *124*, 9048. (h) Zhang, Z.; Berg, A.; Levanon, H.; Fessenden, R. W.; Meisel, D. *J. Am. Chem. Soc.* **2003**, *125*, 7959. (i) Edwards, T. E.; Okonogi, T. M.; Robinson, B. H.; Sigurdsson, S. T. *J. Am. Chem. Soc.* **2001**, *123*, 1527. (j) Verma, S.; Eckstein, F. *Annu. Rev. Biochem.* **1998**, *67*, 99. (k) Kocherginsky, N., Swartz, H. M., Eds. *Nitroxide Spin Labels, Reactions in Biology and Chemistry*; CRC Press: Boca Raton, 1995.
(8) Knauer, B. R.; Napier, J. J. *J. Am. Chem. Soc.* **1976**, *91*, 4395.

10.1021/ja0574872 CCC: $33.50

lighted by Majda and co-workers,[10] who investigated aqueous vapor/liquid interfaces exploiting the redox properties of a nitroxide probe and obtained a satisfactory interpretation of experimental results by means of quantum chemical calculations of water−nitroxide interactions. However, the authors pointed out that a deeper analysis would have required reliable theoretical descriptions of the dynamics of nitroxide-probe molecules in solution, which are, unfortunately, still lacking.

During the last two decades the physics and the chemistry of aqueous solutions have been challenging theoretical and computational chemists.[11] The increasing technology of modern computing facilities and the development of effective and reliable computational methods provided experimental chemists with invaluable tools for the analysis and validation of experimental data, in particular for those collected with modern spectroscopic techniques.[12] In many cases, the accuracy of computed spectroscopic data for little-to-medium sized molecules in the gas phase is comparable to that of their experimental counterparts.[13] Nevertheless, experimental spectroscopic efforts are mostly devoted to condensed-phase systems. Therefore, providing an integrated and easy-to-use computational approach for spectroscopic properties in solution became a natural step toward filling the gap between *in vitro* and *in silico* chemistry.

Many different models have been proposed for taking into account the solvent medium in quantum chemical calculations.[14] In recent years, continuum solvent models have enjoyed considerable success thanks to their reliability coupled to computational effectiveness. Here we will be concerned, in particular, with the polarizable continuum model (PCM),[15] whose latest developments resulted in a linear scaling algorithm fully integrated with several quantum mechanical approaches.[16] The model consists of embedding the solute molecule into a cavity made by enveloping atom-centered spheres whose radii have been parametrized for reproducing experimental solvation free energies;[17] inside the cavity, the relative dielectric constant has the same value as that in a vacuum ($\epsilon = 1$), and it goes steeply to the solvent bulk value ($\epsilon = 78.4$ for water) outside. The presence of the solute perturbs the polarizable medium, which undergoes new equilibration acting back onto the solute molecular parameters by means of an effective reaction field. Such phenomenon is described by the PCM in terms of a pattern of effective charges on the cavity surface.

Despite the very good results on dielectric-dependent molecular properties, many tests have pointed out the limits of PCM in reproducing strong solute−solvent interactions related to intermolecular hydrogen bonding.[18] This problem could be effectively solved by combining a cluster model including the solute and its closest solvent molecules with the PCM description of solvent bulk.[18] Such a discrete-continuum scheme takes into account the quantum chemical nature of short-range effects, the hydrogen bonding, and the classical Coulombic long-range effects by means of the PCM dielectric continuum model. Unfortunately, the cluster or supramolecular frame needs to be sampled onto the configuration space of the solute−solvent system. This means that the geometries of the solute and its closest solvent molecules must be statistically averaged among the energetically accessible configurations of the system. Thus, the efficiency of the sampling methods becomes crucial for the accuracy of quantum chemical calculations.

As part of an ongoing research project, we recently proposed an integrated scheme that combines the cluster-PCM approach and Car−Parrinello[19] molecular dynamics for the calculation of UV and NMR spectroscopic parameters in solution.[20] The focus of the present article is, instead, a stable organic free radical, di-*tert*-butyl nitroxide (DTBN), in aqueous solution, thus extending and tuning the proposed approach to electron paramagnetic resonance (EPR) observables, namely the hyperfine coupling constants (*hcc*) and the **g** tensor. Again, the theoretical machinery for computing EPR molecular parameters has been well established for isolated molecules,[21] but despite some interesting proposals,[22] a definite and unique protocol for taking "quantitatively" into account the many subtle effects of the solvent medium is still lacking.

To overcome the limitations of current empirical force field parametrizations, here we present Car−Parrinello molecular dynamics (CPMD) simulations of a real-size nitroxide radical in aqueous solution; for comparison in the gas phase we carried out a detailed analysis of the internal dynamics of the DTBN molecule going from gas phase to aqueous solution. In addition a dynamical picture of the DTBN−water hydrogen bonding network is provided and compared to the results of standard interaction-energy calculations based on rigid optimized structures. A consistent number of frames, extracted from the trajectories, have been employed for computing DTBN magnetic properties; the availability of several experimental[8,22] and quantum mechanical (QM)[23,24] studies for the EPR parameters of the DTBN−water system allowed us to compare directly the results issuing from CPMD simulations to their experimental and static QM counterparts. The proposed *a posteriori* calculations of spectroscopic properties, compared to other *on-the-fly*

(9) Tedeschi, A. M.; D'Errico, G.; Busi, E.; Basosi, R.; Barone, V. *Phys. Chem. Chem. Phys.* **2002**, *4*, 2180.
(10) Wu, D. G.; Malec, A. D.; Head-Gordon, M.; Majda, M. *J. Am. Chem. Soc.* **2005**, *127*, 4490.
(11) (a) Garrett, B. C.; et al. *Chem. Rev.* **2005**, *105*, 355. (b) Wernet, P.; et al. *Science* **2004**, *304*, 995.
(12) (a) Goedecker, S.; Scuseria, G. E. *Comput. Sci. Eng.* **2003**, *5*, 14. (b) Scuseria, G. E. *J. Phys. Chem. A* **1999**, *103*, 4782. (c) Merchan, M.; Serrano-Andres, L.; Fulscher, M. P.; Roos, B. O. *Recent Adv. Comput. Chem.* **1999**, *4*, 161.
(13) (a) Roos, B. O. *Acc. Chem. Res.* 1999, *32*, 137. (b) Helgaker, T.; Jaszunski, M.; Ruud, K. *Chem.* Rev. **1999**, *99*, 293.
(14) (a) Persico, M.; Tomasi, J. *Chem. Re*v. **1994**, *94*, 2027. (b) Cramer, C. J.; Truhlar, D. G. *Chem. Rev.* **1999**, *99*, 2161. (c) Tomasi, J.; Mennucci, B.; Cammi, R. *Chem. Rev.* **2005**, *105*, 2999.
(15) Miertus, S.; Scrocco, E.; Tomasi, J. *Chem. Phys.* **1981**, *55*, 117.
(16) Scalmani, G.; Barone, V.; Kudin, K. N.; Pomelli, C. S.; Scuseria, G. E.; Frisch, M. J. *Theor. Chem. Acc.* **2004**, *111*, 90.
(17) Cossi, M.; Scalmani, G.; Rega, N.; Barone, V. *J. Chem. Phys.* **2002**, *117*, 43.
(18) (a) Adamo, C.; Cossi, M.; Rega, N.; Barone, V. *Theoretical Biochemistry: Processes and Properties of Biological Systems*; Eriksson, L. A., Ed.; Theoretical and Computational Chemistry, Vol. 9; Elsevier: New York, 1999. (b) Cossi, M.; Barone, V. *J. Chem. Phys.* **2000**, *112*, 2427. (c) Cossi, M.; Barone, V. *J. Chem. Phys.* **2001**, *115*, 4708. (c) Adamo, C.; Barone, V. *Chem. Phys. Lett.* **2000**, *320*, 152. (d) Aquilante, F.; Roos, B.; Barone, V. *J. Chem. Phys.* **2003**, *119*, 12323. (e) Koch, A.; Thomas, S.; Kleinpeter, E. *THEOCHEM* **1997**, *401*, 1. (f) Saracino, G. A.; Tedeschi, A.; D'Errico, G.; Improta, R.; Barone, V. *J. Phys. Chem. A* **2002**, *106*, 10700.
(19) Car, R.; Parrinello, M. *Phys. Rev. Lett.* **1985**, *55*, 2471.
(20) Crescenzi, O.; Pavone, M.; De Angelis, F.; Barone, V. *J. Phys. Chem. B* **2005**, *109*, 445.
(21) (a) Kaupp, M.; Bühl, M.; Malkin, V. G. *Calculation of NMR and EPR parameters*; Wiley-VCH: Weinheim, 2004. (b) Neugebauer, J.; Louwerse, M. J.; Belanzoni, P.; Wesolowski, T. A.; Baerends, E. J. *J. Chem. Phys.* **2005**, *123*, 114101.
(22) (a) Kawamura, T.; Matsunami, S.; Yonezawa, T. *Bull. Chem. Soc. Jpn.* **1967**, *40*, 1111. (b) Mukerjee, P.; Ramachandran, C.; Pyter, R. A. *J. Phys. Chem.* **1982**, *86*, 3189 (c) Owenius, R.; Engstrom, M.; Lindgren, M.; Huber, M. *J. Phys. Chem. A* **2001**, *105*, 10967.
(23) Mattar, S. M.; Stephens, A. D. *Chem. Phys. Lett.* **2001**, *347*, 189.
(24) Rinkevicius, Z.; Telyatnyk, L.; Vahtras, O.; Ruud, K. *J. Chem. Phys.* **2004**, *121*, 5051.

approaches,[25] allowed us to exploit different electronic structure methods for the molecular dynamic simulations and the calculation of EPR parameters. In this way, a more accurate treatment for the more demanding molecular parameters, of both first (*hcc*) and second (**g** tensor) order, could be achieved independently of structural sampling methods. Besides, the effectiveness of the level of theory employed in the Car−Parrinello simulations has been tested. Eventually, decoupling of structural, dielectric, and hydrogen bonding contributions to the observed solvent shift of *hcc* and **g** tensor values provides a detailed picture of the physicochemical features to be taken into account when dealing with complex nitroxide−water systems. The vibrational averaging of spectroscopic parameters by means of Car−Parrinello MD for solution bulk is currently widely employed. On the other hand, many different approaches have been proposed for taking into account the solvent for the calculation of spectral parameters after the MD sampling, a description of solvent molecules in terms of partial point charges at the position of atoms being one of the most employed.[26] The exploited charges come usually from molecular mechanics parametrizations (MM), and they may vary among different force fields. In a recent work on a nitroxide model, dimethyl nitroxide (DMNO) in aqueous solution,[27] we tested the consistency of the discrete-continuum approach by comparing the QM/PCM results to full QM calculations and also to the QM/MM approach. As a result of this study, the perturbation of the solvent on the hyperfine coupling constants could be described by means of QM/PCM, provided that a couple of water molecules is explicitly included in the QM calculations; taking into account the first two water molecules close to the nitroxide at a quantum mechanical level is necessary and sufficient for the description of the short-range solvent−solute interactions, while the rest of the solution is acting on the solute only in terms of electrostatic effects. Thus, the PCM and the MM approaches, once averaged over the MD frames, lead to equivalent results. Consequently, the choice between PCM and MM approaches is essentially a matter of taste and has a negligible influence on the final computed results. For consistency with our previous works[20,27,28] we will use here the PCM approach for taking into account bulk solvent effects.

In summary, in the present work we present a validation of the CPMD/QM/PCM approach for predicting the magnetic properties of the DTBN molecule in aqueous solution. Such integration of different theoretical techniques into a unified computational protocol provides a valuable tool for nonspecialists studying complex condensed phase chemical systems.

II. Methods

Car−Parrinello Molecular Dynamics. Within the framework of density functional theory (DFT),[29] the Car−Parrinello (CP) extended-Lagrangian scheme[9] provides a unified and affordable approach for classical molecular dynamic simulation and first-principle electronic structure calculations. Nowadays it has become the method of choice for investigating the dynamics of condensed phases, in solid-state physics as well as in soft matter chemistry.[30] The details of the theory and the implementation of the Car−Parrinello method are well reviewed in recent literature.[31,32] In the present paper, gas-phase and aqueous-solution CP molecular dynamic simulations were carried out using the parallel version[32] of the original CP code[33] and the PBE density functional.[34] The wave functions (density) were expanded in a plane-wave basis set up to an energy cutoff of 25 (200) Ry; core states are projected out using "ultra-soft" pseudopotentials generated according to the Vanderbilt method.[35] Equations of motion were integrated using a time step of 10 au (0.242 fs) with a fictitious electron mass $\mu =$ 1000 au. For the system in aqueous solution, the initial configuration was obtained by replacing six water molecules by a DTBN molecule from a previously equilibrated liquid water trajectory obtained for a constant-volume cubic supercell including 64 water molecules at a density of 1.00 g/cm^3.[36] The simulation in a vacuum was performed, instead, starting from the optimized structure of DTBN. The considered systems have been equilibrated for 1.5 ps, applying a Nosé thermostat,[37] which ensures a canonical (NVT) ensemble. After equilibration, the systems have been observed for a total time of 4.0 ps, during which statistical averages were taken. The average temperatures during the dynamics simulations in vacuo and in solution were 307 and 318 K, respectively. The present methodology has been recently shown[36] to provide radial distribution functions of liquid water in good agreement with experimental data[38,39] and with previous ab initio molecular dynamics simulations by Silvestrelli and Parrinello.[40,41]

Cluster Calculations. Calculations of optimized structural parameters were carried out by the GAUSSIAN03 package.[42] The DTBN geometry was fully optimized using the PBE exchange and correlation functional both in its pure GGA formalism[34] and within the hybrid Hartree−Fock-DFT scheme known as PBE0.[43] Moreover, we performed several tests up to convergence of geometrical parameters exploiting both valence-double-ζ and valence-triple-ζ sets, augmented by diffuse and polarization functions, from the Pople[44] and Dunning series.[45] The 6-311++G(3df,2pd) basis set was found to achieve a good convergence while remaining relatively cheap. Employing such a basis set together with the PBE0 functional we calculated the minimum energy structure of DTBN and its adducts involving a single and a double H-bond with water molecules; at the same level of theory we computed, for comparison, the water molecule and its dimer. All these geometry optimizations were carried out with and without the PCM description

(25) (a) Aschi, M.; Spezia, R.; Di Nola, A.; Amadei, A. *Chem. Phys. Lett.* **2001**, *344*, 374. (b) R. Spezia, R.; Aschi, M.; Di Nola, A.; Amadei, A. *Chem. Phys. Lett.* **2002**, *365*, 450. (c) Amadei, A.; Marinelli, F.; D'Abramo, M.; D'Alessandro, M.; Anselmi, M.; di Nola, A.; Aschi, M. *J. Chem. Phys.* **2005**, *122*, 124506. (d) Sebastiani, D.; Parrinello, M. *J. Phys. Chem. A* **2001**, *105*, 1951.

(26) (a) Bühl, M. *J. Phys. Chem. A* **2002**, *106*, 10505 (b) Asher, J. R.; Doltsinis, N. L.; Kaupp, M. *J. Am. Chem. Soc.* **2004**, *126*, 9854 (c) Bühl, M.; Parrinello, M. *Chem. Eur. J.* **2001**, *7*, 4487. (d) Bühl, M. *Inorg. Chem.* **2005**, *44*, 6277. (e) Aidas, K.; Kongsted, J.; Osted, A.; Mikkelsen, K. V.; Christiansen, O. *J. Phys. Chem. A* **2005,** 109, 8001**.**

(27) Pavone, M.; Benzi, C.; De Angelis, F.; Barone, V. *Chem. Phys. Lett.* **2004**, *395*, 120.

(28) (a) Saracino, G. A. A.; Tedeschi, A.; D'Errico, G.; Improta, R.; Barone, V. *J. Phys. Chem. A* **2002**, *106*, 10700. (b) Improta, R.; Barone, V. *J. Am. Chem. Soc.* **2004**, *126*, 14320. (c) Cimino, P.; Barone, V. *THEOCHEM* **2005**, *729*, 1.

(29) (a) Hohenberg, P.; W. Kohn, W. *Phys. Rev.* **1964**, *136*, B864. (b) Kohn, W.; Sham, L. J. *Phys. Rev.* **1965**, *140*, A1133.

(30) (a) Kanai, Y.; Cicero, G.; Selloni, A.; Car, R.; Galli, G. *J. Phys. Chem. B* **2005**, *109*, 13656 (b) Fischer, D.; Curioni, A.; Billeter, S. R.; Andreoni, W. *Phys. Rev. Lett.* **2004**, *92*, 236405. (c) Gleich, D.; Hutter, J. *Chem. Eur. J.* **2004**, *10*, 2435.

(31) (a) Andreoni, W.; Curioni, A. *Parallel Comput.* **2000**, *26*, 819. (b) Hutter, J.; Curioni, A. *ChemPhysChem* **2005**, *6*, 1.

(32) Giannozzi, P.; De Angelis, F.; Car, R. *J. Chem. Phys.* **2004**, *120*, 5903.

(33) Pasquarello, A.; Laasonen, K.; Car, R.; Lee, C.; Vanderbilt, D. *Phys. Rev. Lett.* **1992**, *69*, 1982.

(34) Perdew, J. P.; Burke, K.; Ernzerhof, M. *Phys. Rev. Lett.* **1996**, *77*, 3865.

(35) Vanderbilt, D. *Phys. Rev. B* **1990**, *41*, 7892.

(36) Hetenyi, B.; De Angelis, F.; Giannozzi, P.; Car, R. *J. Chem. Phys.* **2004**, *120*, 8632.

(37) Nosé, S. *J. Chem. Phys.* **1984**, *81*, 511.

(38) Hura, G.; Sorenson, J. M.; Glaeser, R. M.; Head-Gordon, T. *J. Chem. Phys.* **2000**, *113*, 9140.

(39) Soper, A. K. *Chem. Phys.* **2000**, *258*, 121.

(40) Silvestrelli, P. L.; Parrinello, M. *J. Chem. Phys.* **1999**, *111*, 3572

(41) Silvestrelli, P. L.; Parrinello, M. *Phys. Rev. Lett.* **1999**, *82*, 3308.

(42) Frisch, M. J.; et al. *Gaussian03*, rev. C.02; Gaussian. Inc.: Philadelphia, PA, 2003.

(43) Adamo, C.; Barone, V. *J. Chem. Phys.* **1999**, *110*, 6158.

(44) Francl, M. M.; Petro, W. J.; Hehre, W. J. S.; Binkley, J.; Gordon, M. S.; DeFrees, D. J.; Pople, J. A. *J. Chem. Phys.* **1982**, *77*, 3654.

(45) Dunning, T. H., Jr. *J. Chem. Phys.* **1989**, *90*, 1007.

of solution bulk. Single-point energy calculations and magnetic properties were also evaluated for comparison to the MD averaged results.

Magnetic Properties. All the calculations of magnetic properties were carried out by the GAUSSIAN03 package.[42]

The *hcc*'s are proportional to the electron spin density ρ_S at or near the position of any magnetic nucleus. In the present work we will only consider the isotropic Fermi contact term at the nitrogen nucleus, which is given by:

$$A_N = \frac{8\pi}{3} g_n g_e \mu_n \mu_e \rho_s (r_N) \quad (1)$$

where μ_n and g_n are respectively the magneton and the g factor of the nucleus, μ_e is the Bohr magneton and g_e is the g value for the electron; finally $\rho_S(r_N)$ is the electron spin density at the nitrogen nuclear position. DFT computations were performed at the PBE0 level of theory by using the purposely tailored EPR-II basis sets.[46,47] Quadratic configuration interaction single and double (QCISD) calculations were also performed with the basis set purposely tailored by Chipman for evaluation of EPR parameters.[48] Thus, we combined the DFT description of the nitroxide system with a more accurate and correlation-consistent method for computing the magnetic properties; from the total system a model region is extracted, where the QCISD calculation was carried out and the resulting data were combined as follows: $A_N = A_N^{DFT}$(total system) + A_N^{QCISD}(model system) − A_N^{DFT}(model system). Such an approach has already been proven to be particularly efficient in the calculation of nitroxide hyperfine coupling constants.[2]

For what concerns the **g** tensor, we will refer to shifts with respect to the free-electron value ($g_e = 2.002319$) which can be dissected into three main contributions:[49,50]

$$\Delta g = \Delta g^{RMC} + \Delta g^{GC} + \Delta g^{OZ/SOC} \quad (2)$$

Δg^{RMC} and Δg^{CC} are first-order contributions, which take into account relativistic mass (RMC) and gauge (GC) corrections, respectively. The first term can be expressed as:

$$\Delta g^{RMC} = -\frac{\alpha^2}{S} \sum_{\mu,\nu} P_{\mu,\nu}^{\alpha-\beta} \langle \varphi_\mu | \hat{T} | \varphi_\nu \rangle \quad (3)$$

where α is the fine structure constants, S the total spin of the ground state, $P_{\mu,\nu}^{\alpha-\beta}$ is the spin density matrix, $\{\varphi\}$ the basis set and $\hat{T}$ is the kinetic energy operator.

The second term is given by:

$$\Delta g^{GC} = -\frac{1}{2S} \sum P_{\mu,\nu}^{\alpha-\beta} \langle \varphi_\mu | \sum_A \xi(r_A) [\vec{r}_A \vec{r}_0 - \vec{r}_{A,r} \vec{r}_{0,s}] \hat{T} | \varphi_\nu \rangle \quad (4)$$

where $\vec{r}_A$ is the position vector of the electron relative to the nucleus A, $\vec{r}_A$ the position vector relative to the gauge origin and $\xi(r_A)$, depending on the effective charge of the nuclei, will be defined below. These two terms are usually small and have opposite signs so that their contributions tend to cancel out.

The last term in eq 2, $\Delta g^{OZ/SOC}$, is a second-order contribution arising from the coupling of the orbital Zeeman (OZ) and the spin−orbit coupling (SOC) operators. The OZ contribution is:

$$\hat{H}_{OZ} = \beta \sum_i \vec{B} \vec{l}(i) \quad (5)$$

It shows a gauge origin dependence, arising from the angular momentum of the ith electron, $\vec{l}(i)$. In our calculations a gauge including atomic orbital (GIAO) approach is used to solve this dependence.[51,52]

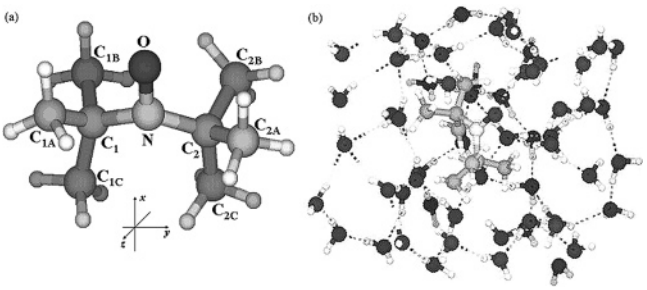

Figure 1. (a) Structure and labeling of di-*tert*-butyl nitroxide (DTBN) and orientation. (b) Super-cell unit consisting of one DTBN and 58 water molecules for aqueous solution dynamics.

Finally the SOC term is a true two-electron operator, but here it will be approximated by a one-electron operator involving adjusted effective nuclear charges. This approximation has been proven to work fairly well in the case of light atoms, providing results close to those obtained using more refined expressions for the SOC operator.[53] The one-electron approximate SOC operator reads:

$$\hat{H}_{SOC} = \sum_{A,i} \xi(r_{i,A}) \vec{l}_A(i) \vec{s}(i) \quad (6)$$

where $\vec{l}_A(i)$ is the angular momentum operator of the ith electron relative to the nucleus A and $\vec{s}_A(i)$ its spin-operator. The function $\xi(r_{i,A})$ is defined as:[54]

$$\xi(r_{i,A}) = \frac{\alpha^2}{2} \frac{Z_{eff}^A}{|\vec{r}_i - \vec{R}_A|^3} \quad (7)$$

where Z_{eff}^A is the effective nuclear charge of atom A at position $\vec{R}_A$.

Spin-unrestricted calculations were performed providing the KS zero-order molecular orbitals. The magnetic field dependence has been taken into account using the coupled-perturbed KS formalism similarly as described by Neese,[51] but including the GIAO approach.[52,55] Solution of the coupled perturbed KS equation (CP−KS) leads to the determination of the OZ/SOC contribution.

As for hyperfine coupling constants, calculations of **g** tensor were carried out at the PBE0 level of theory employing the EPR-II basis set; such approach has been proven to be very efficient for DFT-GIAO calculations of magnetic properties.[55] Bulk solvent effects have been taken into account by the PCM, using the UAHF parametrization of atomic-group sphere radii.[56]

Both in the gas phase and in aqueous solution the radical motion is fast enough to lead to complete rotational averaging, so that the quantity directly related to experiment is actually $\Delta g_{iso} = {}^1/_3 Tr(\mathbf{g} - g_e)$ and we will consider in the following only this value.

III. Results

Car−Parrinello Molecular Dynamics. Structure, labeling, and orientation of di-*tert*-butyl nitroxide (DTBN) are shown in Figure 1a together with the periodic super-cell employed for the aqueous solution molecular dynamics, Figure 1b. Average geometrical parameters of the DTBN molecule from the Car−Parrinello MD simulations in gas phase and in aqueous solution

(46) Adamo, C.; Barone, V.; Fortunelli, A. *J. Chem. Phys.* **1995**, *102*, 384.
(47) Barone, V. *Theor. Chim. Acta* **1995**, *91*, 113.
(48) Chipman, D. M. *Theor. Chim. Acta* **1992**, *82*, 93.
(49) McWeeny, R. *Methods of Molecular Quantum Mechanics*; Academic Press: London, 1992.
(50) Stone, A. J. *Proc. R. Soc. London, Ser. A* **1963**, *271*, 424.
(51) Neese, F. *J. Chem. Phys.* **2001**, *115*, 11080.
(52) (a) Ditchfield, R. *Mol. Phys.* **27**, *789* 1974. (b) Cheesman, J. R.; Trucks, G. W.; Keith, T. A.; Frisch, M. J. *J. Chem. Phys.* **1998**, *104*, 5497.
(53) Malkina, O. L.; Vaara, J.; Schimmelpfenning, B.; Munzarova, M. L.; Malkin, V. G.; Kaupp, M. *J. Am. Chem. Soc.* **2000**, *122*, 9206.
(54) Koseki, S.; Schmidt, M. W.; Gordon, M. S. *J. Phys. Chem.* **1992**, *96*, 10768.
(55) (a) Ciofini, I.; Adamo, C.; Barone, V. *J. Chem. Phys.* **2004**, *121*, 6710. (b) Barone, V.; Carbonniere, P.; Pouchan, C. *J. Chem. Phys.* **2005**, *122*, 224308.
(56) Barone, V.; Cossi, M.; Tomasi, J. *J. Chem. Phys.* **1997**, *107*, 3210.

Table 1. Average Geometrical Parameters of DTBN from CPMD Simulations: Bond Distances (Å), Angles and Dihedrals (deg), Standard Deviations in Parentheses

	gas phase	aqueous solution
NO	1.30 (0.02)	1.31 (0.02)
NC_X [a]	1.53 (0.04)	1.54 (0.06)
C_XC_{XY} [ab]	1.55 (0.04)	1.55 (0.04)
C_1NC_2	128 (3)	127 (4)
ONC_X [a]	114 (4)	115 (4)
abs(C_1NOC_2)	166 (8)	170 (8)

[a] $X = 1, 2$. [b] $Y =$ A, B, C.

Table 2. Main Characteristics of DTBN−H_2O Hydrogen Bonds from CPMD Simulations: Bond Lengths (Å), Angles (deg), Standard Deviations in Parentheses

average number of H-bonds	1.2 (0.5)
% 0 H-bond	7%
% 1 H-bond	63%
% 2 H-bond	30%
$O_{DTBN}\cdots O_{water}$	2.9 (0.2)
$O_{DTBN}\cdots H_{water}$	1.9 (0.3)
$O_{DTBN}\cdots O_{water}-H_{water}$	15 (7)

are listed in Table 1. Only very small variations of the average structure occurred when going from gas phase to aqueous solution involving essentially lengthening of the NO bond and increasing of the CNOC improper dihedral. A picture of the gas-phase and aqueous-solution DTBN dynamics is provided by the distribution functions along the trajectories of the N−O bond length (Figure 2a) and CNOC improper dihedral (Figure 2b). Concerning the NO bond, both plots present a similar trend, although the peak is sharper in gas phase than in solution, in close agreement with the above-mentioned lengthening of the average value. On the other hand, the distribution of the CNOC improper dihedral angle (related to the out-of-plane motion of the nitroxide backbone) in the gas phase shows two equivalent peaks symmetric with respect to a planar configuration, whereas in aqueous solution there is only one well-defined maximum corresponding to a planar arrangement of the CNOC moiety. In agreement with former theoretical predictions about DTBN in the gas phase,[23,24] the two symmetric maxima of the gas-phase CNOC dihedral distribution are indicative of two equivalent nonplanar minima and of a smooth potential energy surface governing the out-of-plane motion of the NO moiety. Therefore, the non-negligible probability of finding the DTBN molecule close to a planar configuration in the gas phase should be taken into account. Such an issue is even more crucial in the case of the aqueous solution dynamics. The water medium enhances

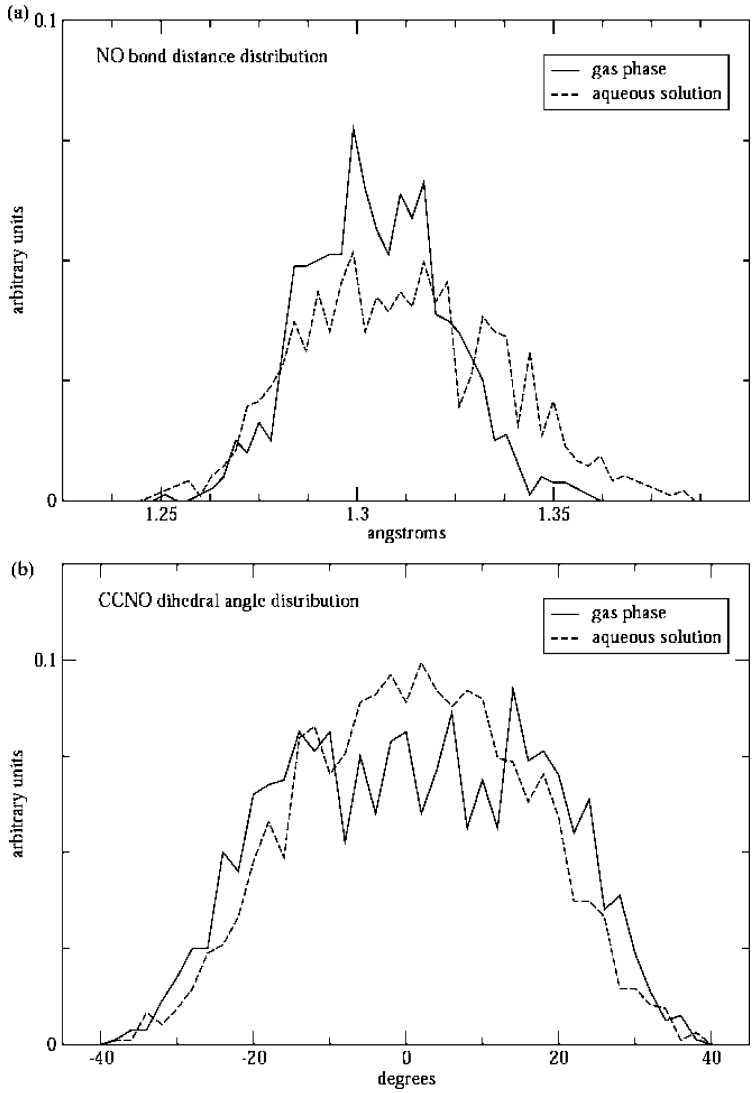

Figure 2. Distributions of NO bond length (a) and C_1NOC_2 dihedral angle from CPMD trajectories (b).

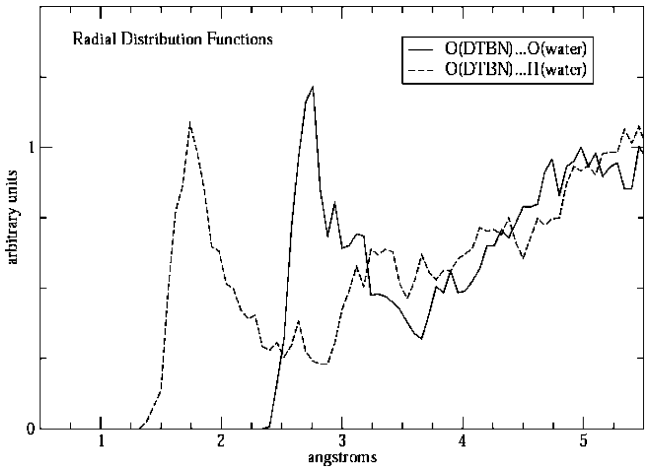

Figure 3. Radial distribution functions $O_{DTBN}-O_{water}$ (full line) $O_{DTBN}-H_{water}$ (dashed line).

the flexibility of the CNOC dihedral angle, and the large peak centered at 0° is the result of the ease with which the NO moiety undergoes inversion.

The structure of the solvation sphere of the DTBN molecule in aqueous solution was analyzed in terms of the following simple standard criteria for hydrogen bonds:[26,57]

$$\begin{aligned} \text{dist}(O_{DMNO}\cdots O_{WATER}) &\le 3.5\ \text{Å} \\ \text{dist}(O_{DMNO}\cdots H_{WATER}) &\le 2.6\ \text{Å} \\ \text{angle}(O_{DMNO}\cdots O_{WATER}-H_{WATER}) &\le 30° \end{aligned} \qquad (8)$$

Table 2 lists the results of this analysis. The average number of DTBN−water H-bonds is 1.2, and the average H-bonding structural parameters are in close agreement with the maximum peaks of the radial distribution functions (RDF) shown in Figure 3.

The average number of H-bonds is significantly below the value of two suggested by experimental results for some spin probes and actually found in the simple DMNO model.[26] As a matter of fact, the presence of two bulky *tert*-butyl groups embedding the nitroxide moiety plays a key role in determining the space available to the solvent molecules accessing the DTBN oxygen atom. This is well evidenced by the average CNC angle, which is around 115° in DMNO (as well as in the most widely used spin probes) and around 128° in DTBN; thus, in the latter case the methyl groups are pushed up, crowding the available space around the oxygen atom. Nevertheless, also in DTBN aqueous solution there is a significant number of structures (30%) characterized by two genuine solute−solvent hydrogen bonds, thus indicating that a proper dynamical average is needed to compute reliable spectroscopic parameters in solution.

Cluster Calculations. Because of the lack of any experimental structure of the DTBN molecule, we must trust first-principle geometry optimizations. In this case we employed the PBE0 functional which also provides very good geometrical results for a wide range of organic free-radical species.[11] To minimize the differences between plane waves and Gaussian type orbital (GTO) approaches, we tested a number of basis sets with respect to the most important geometrical parameters of the DTBN radical. Table 3 lists the results obtained with different and very large basis sets and shows that the 6-311++G(3df,2pd) basis set represents a very good compromise between reliability and computational burden. As a consequence, all the geometry optimizations have been carried out with this basis set. To quantify the effect of the exchange contribution on the geometry we carried out a geometry optimization of the DTBN isolated molecule at the PBE and PBE0 levels of theory, obtaining the results listed in Table 4. As a matter of fact, the conventional GGA functional (PBE) overestimates the NO bond length; this behavior is quite general for GGA models and can be partially corrected by the inclusion of an amount of nonlocal Hartree−Fock (HF) exchange.[2,20] The CNC valence angle and the out-of-plane distortion of the NO moiety are much less sensitive to the form of the density functional. Dynamical effects on the geometry of DTBN are evidenced by comparison between the average structure along the gas-phase CPMD trajectory and the PBE energy minimum. Since the employed GTO basis set is at convergence with respect to the geometrical parameters, we think it is reasonable to compare these two data sets. As a matter of fact the minimum and the average dynamical structures are in pretty good agreement, and the very small differences (within the standard deviations) are in the range of reasonable vibrational contributions.

Furthermore, we performed a calculation of the geometrical structure of the DTBN−$(H_2O)_n$ (n = 0, 1, 2) with and without the PCM for modeling the solvent bulk. Table 5 lists the results on structural and magnetic properties. Interestingly, there is a very small shift of geometrical parameters going from gas phase to solution minima; the trend of the NO bond displacements going from DTBN to DTBN−(H_2O) and to DTBN−$(H_2O)_2$ is the same in the gas phase and in PCM embedded structures. Eventually, to have a flavor of the energies involved in

Table 3. Test of Basis Set Convergence, for Geometry Optimization, at the PBE0 Level of Theory: Bond Lengths (Å), Angles and Dihedrals (deg)

basis functions		DTBN geometrical parameters		
		N–O	C–N–C	C–N–O···C
6-31G(d)	186	1.276	127.6	160.9
6-31+G(d,p)	280	1.277	127.5	161.4
6-311G(d)	234	1.270	127.3	161.0
6-311+G(d,p)	328	1.272	127.3	161.6
6-311++G(2d,2p)	450	1.271	127.3	161.7
6-311++G(3df,2pd)	660	1.268	127.3	161.8
cc-pVDZ	230	1.271	127.5	161.0
cc-pVTZ	552	1.270	127.4	162.0
aug-cc-pVTZ	874	1.269	127.3	162.1
cc-pVQZ	1090	1.268	127.3	162.0

Table 4. Geometric (Bond Lengths in Å and Angles in Degrees) and Magnetic (A_N in Gauss and Δg_{iso} in ppm) Properties of DTBN Computed at the PBE and PBE0 Levels

	PBE	PBE0
	Geometric[a]	
N−O	1.284	1.268
C−N−C	127.0	127.3
C−N−O···C	160.8	161.8
	Magnetic	
A_N[b]	13.04	12.28
Δg_{iso}[b]	3823	3736

[a] 6-311++G(3df,2pd) basis set. [b] Single-point PBE0/EPR-II property evaluation.

(57) Ferrario, M.; Haughney, M.; McDonald, I. R.; Klein, M. L. *J. Chem. Phys.* **1990**, *93*, 5156.

Table 5. Structural and Magnetic Parameters Computed for DTBN and Its Water Adducts in Vacuum and with a PCM Representation of Solvent Bulk; Bond Lengths in Å, Valence and Dihedral Angles in Degrees, Energies in kcal/mol, A_N in Gauss and Δg_{iso} in ppm

	in a vacuum geometry optimization.			geometry optimization with PCM		
	DTBN	DTBN(H_2O)	DTBN(H_2O)$_2$	DTBN	DTBN(H_2O)	DTBN(H_2O)$_2$
			Geometric[a]			
N−O	1.268	1.269	1.271	1.270	1.271	1.273
C−N−C	127.3	127.4	127.8	127.1	127.3	128.0
C−N−O···C	161.8	163.1	164.5	163.3	163.6	165.2
O···O$_{water}$	−	2.821	2.889	−	2.806	2.867
O···H$_{water}$	−	1.856	1.947	−	1.835	1.922
O···O−H$_{water}$	−	7.9	10.5	−	0.5	10.4
			A_N[b]			
no PCM	12.28	12.74	13.51	−	−	−
PCM	13.06	13.31	14.06	12.77	13.22	13.91
			Δg_{iso}[b]			
no PCM	3736	3502	3304	−	−	−
PCM	3591	3397	3222	3574	3396	3211

[a] PBE0/6-311++G(3df,2pd) level of theory. [b] PBE0/EPR−II level of theory, PCM radii = UAHF.

Table 6. Relative Interaction Energies (kcal/mol) of DTBN−H_2O, DTBN−(H_2O)$_2$, and H_2O−H_2O; Single Points at the PBE0/6-311++G(3df,2pd) Level of Theory on Optimized Geometries

structure/ single point	gas phase/ gas phase	gas phase/ PCM	PCM/ PCM
H_2O−H_2O	−4.5	−2.1	−2.5
DTBN−H_2O	−5.7	−1.4	−1.2
DTBN−(H_2O)$_2$[a]	−12.3 (−6.6)	−0.5 (0.9)	−0.9 (0.3)

[a] The energetic contribution of the second DTBN−H_2O H-bond is given in parentheses.

nitroxide−water interaction we carried out single-point calculations on the structures optimized in the gas phase for the above-mentioned adducts and for the water dimer again at the PBE0/6-311+G(3df,2pd) level (see Table 6). In the gas phase both the first and second nitroxide−water H-bonds provide an energetic balance (−5.7 and −6.6 kcal/mol, respectively) more favorable than that of solvent−solvent interaction (−4.5 kcal/mol for the H_2O dimer). The situation changes taking the solvent bulk into account, since now the energy corresponding to the water dimer, −2.1 kcal/mol, is larger than those of both DTBN−water clusters, −1.4 and −0.5 kcal/mol, respectively. Furthermore, the contribution of the second H-bond is now energetically unfavorable, 0.9 kcal/mol and the whole trend is confirmed also taking into account the solvent in the geometry optimizations. Remarkably, all these results are consistent with the H-bonding analysis of the aqueous solution trajectories where for the most part of the time there is just one DTBN−water H-bond.

Magnetic Properties. To achieve a consistent level of theory for the prediction of hyperfine coupling constants we performed a series of calculations with several basis sets; Table 7 lists the computed A_N on a single DTBN structure extracted from the gas-phase CPMD simulation. As is well-known, none of the density functionals proposed until now allows a quantitative evaluation of A_N's.[2] Thus, we followed the aforementioned QCISD-DFT approach, sketched in Figure 4 and already tested and validated for a large series of nitroxide radicals.[2] In particular, the PBE0 hybrid functional and the EPR-II basis set were used for most of the calculations, and the QCISD correction was only computed for the DTBN gas-phase equilibrium value. In other words, in the present work the dynamical effect on the *hcc* was computed at the PBE0 level of theory by averaging the values obtained along the CPMD trajectories. To this end we extracted equal time-spaced structures of DTBN

Table 7. Test of Basis Set Convergence, for Hyperfine Coupling Constant Calculations, at the PBE0 Level of Theory; A_N Values in Gauss; Values Computed on a DTBN Geometry Randomly Extracted from the Gas-Phase Car−Parrinello Dynamics

basis functions		A_N
6-31G(d)	186	15.73
6-31+G(d,p)	280	15.57
6-311G(d)	234	12.55
6-311+G(d,p)	328	12.68
EPR-II	296	14.32
EPR-III	598	14.33
cc-pVDZ	230	16.73
cc-pVTZ	552	11.31
aug-cc-pVTZ	874	11.02

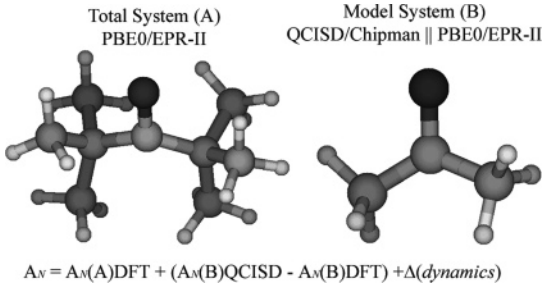

Figure 4. Scheme of the combined QCISD-DFT approach for the calculation of A_N.

(for the gas phase) and DTBN−(H_2O)$_2$ (for the aqueous solution) along the CPMD trajectories, and we repeated on each of these frames a calculation of the EPR spectral observables. Since, as mentioned in the preceding section, the number of water−nitroxide hydrogen bonds in individual CPMD frames ranges from zero to two, we extracted from the aqueous solution trajectory clusters containing the solute plus the two water molecules closest to the nitroxide oxygen, the rest of the solvent being well described by the PCM. This should be considered a general procedure derived from the H-bond analysis that has been validated in previous studies about other molecules involving oxygen atoms.[20,27] Figure 5 shows the A_N values in gas phase (a) and in aqueous solution (b) as well as the Δg_{iso} values (c,d) computed along the trajectories together with the average value; it is quite apparent that 200 frames are largely sufficient to obtain well-converged average results. Table 8 lists the data obtained from the Car−Parrinello dynamics. Structural modifications induced by the solvent (collectively referred to

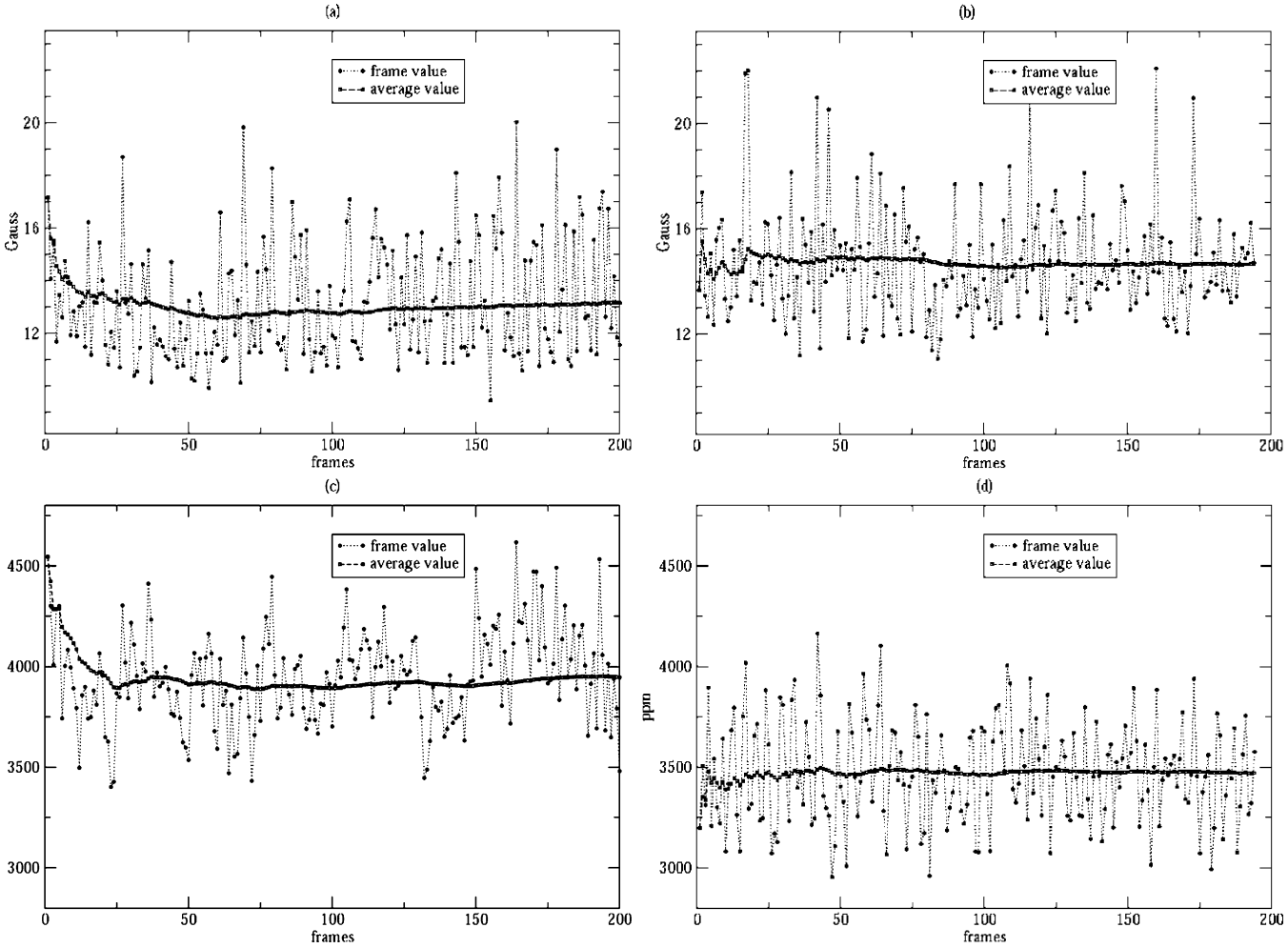

Figure 5. Convergence of A_N (in Gauss) and Δg_{iso} (in ppm) computed along the CPMD trajectories: (a) A_N in gas phase; (b) A_N in aqueous solution; (c) Δg_{iso} in gas phase; (d) Δg_{iso} in aqueous solution.

Table 8. Average Values of A_N (in Gauss) and Δg_{iso} (in ppm) Computed at the PBE0/EPR-II Level of Theory Using Structures Issuing from CPMD Simulations; Standard Deviations Are Given in Parentheses

	A_N	Δg_{iso}
	Gas Phase	
DTBN	13.1 (0.2)	3946 (17)
exp [a,b]	15.5	
	Aqueous Solution	
DTBN	12.6 (0.2)	3913 (27)
DTBN−$(H_2O)_2$	14.7 (0.2)	3471 (18)
exp[a,d]	17.17	3241
	Solvent Shifts	
CPMD	1.6	−475
exp[a]	1.7	−

[a] Reference 19. [b] Derived by a linear unweighted least-squares fitting of the DTBN A_N in 31 different solvents related to the solvent dielectric constants. [c] DTBN−$(H_2O)_2$ clusters extracted from the MD plus the PCM for solvent bulk. [d] Reference 22.

as indirect solvent effect) do not affect very much the *hcc* and **g** tensor values, the spectral parameters computed on the isolated solute as extracted from the aqueous solution dynamics differing by 0.5 G and 33 ppm from the average values obtained from the gas phase. On the other hand, direct solvent shifts (related to solute polarization at constant geometry) are significant; interestingly, the water environment enforces the hyperfine splitting in an opposite direction than the structural effect, whereas it decreases the value of the **g** tensor shift following the same trend of the indirect solvent effect. To the best of our knowledge there is no value for the **g** tensor of DTBN in gas phase, whereas estimates of A_N *in a vacuum* have been obtained by extrapolation from experimental data in different solvents.[8] The CPMD average results are pretty far from reproducing absolute experimental data, but the A_N solvent shift is in very good agreement with its experimental counterpart. This failure in the reproduction of absolute data from CPMD simulation is related to the level of theory employed for the molecular dynamic simulations; as a matter of fact, the use of plane-wave basis sets for the CPMD simulation prevents the calculation of nonlocal HF exchange with an affordable computational cost. Conventional GGA functionals, employed in CPMD, provide equilibrium structures that are less accurate than those obtained from hybrid HF/KS models, and this limitation affects also the MD trajectories and consequently the MD averaged spectroscopic values.[58] The effect of the exchange functional on the accuracy of the computed spectroscopic data can be highlighted by looking at the differences between PBE and its hybrid counterpart, PBE0, in calculating the structural and magnetic properties of the isolated DTBN molecule; the results are listed in Table 4. As a matter of fact, compared to the more reliable

(58) Pavone, M.; Barone, V.; Ciofini, I.; Adamo, C. *J. Chem. Phys.* **2004**, *120*, 9167.

Table 9. EPR Parameters of DTBN in Aqueous Solution; A_N (in Gauss) and Δg_{iso} (in ppm)

	QCISD/DFT +	Δ(dynamics) +	Δ(solvent)	TOTAL	EXP[b,c]
A_N	15.5	0.1	1.6	17.2	17.17
	GIAO-DFT +	Δ(dynamics) +	Δ(solvent)	TOTAL	
Δg_{iso}	3736	123	−475	3348	3241

[a] Solvent shifts, see Table 5. [b] Reference 19. [c] Reference 22.

PBE0, the PBE structure provides a difference of 0.76 G and 87 ppm in the case of A_N and Δg_{iso} values, respectively.

A further analysis can be carried out from the computed EPR values on equilibrium DTBN and DTBN−water cluster geometries, as listed in Table 5. The alternative inclusion of the PCM for the solution bulk and of just two explicit water molecules gives us the chance to decouple the effects of the solvent dielectric properties to those arising from the solute−solvent hydrogen bonding. Concerning A_N, specific interactions (e.g., H-bond) shift the computed value by 0.56 G for the first H-bond and by 1.23 for the second one, whereas the effect of the dielectric contribution goes from 0.78 G when one does not consider any explicit solvent molecule to a value of roughly 0.55 for both the single and double H-bond adducts. Interestingly, considering also the relaxation of the cluster induced by the solvent, the A_N shift from gas phase to aqueous solution (in particular the DTBN$(H_2O)_2$/PCM value) of 1.63 G is close to that obtained from the CPMD average values (1.6 G). There should certainly be an error compensation that leads to results comparable to those obtained by considering the internal finite temperature and solvent motions. As a matter of fact, the Δg_{iso} values computed on cluster structures optimized in gas phase and in solution lead to a solvent shift quite different from that issuing from CPMD trajectories (−525 and −475 ppm, respectively). On the other hand, the dielectric (PCM) effect on both A_N and **g** tensor decreases when explicit solvent molecules are included, thus showing the need of taking both short- and long-range solvent effects into proper account.

Thus, following our previous work on the acetone molecule,[20] we tried to rationalize the computed spectroscopic observations by decoupling the different effects tuning the DTBN molecular properties. We took as the gas-phase reference structure of DTBN the PBE0/6-311++G(3df,2pd) energy minimum; using this geometry we extracted the model where the QCISD/Chipman calculation was carried out, i.e., dimethyl nitroxide kept frozen at the structure of DTBN. The intramolecular dynamics of DTBN has certainly a non-negligible effect on the computed spectroscopic value, which is quantified by the difference between the spectral parameters of the PBE gas-phase minimum and those averaged over the PBE CPMD gas-phase trajectory. The solvent effect was eventually taken into account by comparing the results obtained from the gas-phase and the aqueous-solution dynamics. With this straightforward combination of the computed data, we obtained the nitrogen hyperfine coupling constant and **g** tensor in quantitative agreement with their experimental counterparts. As summarized by Table 9, the computed A_N of 17.2 G is directly comparable to the experimental value of 17.17 G; the computed **g** tensor shift, 3384 ppm, is in close agreement with the experimental one (3241 ppm) with a relative error lower than 5%, which is well within the expected error bar of the DFT/GIAO approach.[51,55]

IV. Conclusions

Nitroxide-labeled molecules are widely employed as effective probes for investigating the properties of complex systems; often the NO moiety experiences the interface among chemically and/or physically inhomogeneous environments, so that the resulting experimental data are not amenable to unambiguous interpretations. In such circumstances, computational investigations can be of invaluable help provided that all the factors determining the overall spectroscopic observable (e.g. spin polarization, vibrational averaging, solute−solvent interactions) are properly taken into account. As a first step in this direction we have chosen to investigate in aqueous solution a prototypical nitroxide radical (DTBN) for which reliable experimental data are available. Our results can be conveniently summarized in terms of the following three main aspects:

(1) Dynamics of the DTBN molecule: both in gas phase and in solution the nitroxide radical is characterized by a remarkable flexibility, whose effect cannot be taken into account by standard models based on "frozen" minimum-energy structures. The probability of finding DTBN in a planar configuration is quite large in solution, even if there is not a well-defined planar energy minimum in the potential energy surface. Furthermore, in gas phase, the most probable configuration of DTBN is significantly pyramidal, in agreement with our and previous static computations;[23] however, a non-negligible probability exists for an effective planar configuration resulting from the rapid inversion of the NO moiety. Vibrational averaging effects due to this large amplitude internal motion have been taken into account by computing EPR data along the CPMD trajectories.

(2) Hydrogen-bonding network around the nitroxide moiety: there is continuing effort aimed at determining the structure of the first solvent shell around nitroxide radicals in hydrogen-bonding solvents. The analysis we have reported relies on both static and dynamic perspectives. Quite surprisingly, most frames of the CPMD trajectory in aqueous solution are characterized by a single DTBN−water H-bond, with a comparatively small contribution of structures with zero or two H-bonds. This finding is at variance with previous computational and experimental works, whose results have been systematically interpreted in terms of a dominant role played by DTBN−$(H_2O)_2$ adducts. To understand such an unexpected trend, we moved back to standard geometry optimizations of suitable clusters. Interestingly, formation of both one and two DTBN−H_2O hydrogen bonds is favored with respect to H_2O−H_2O for gas-phase clusters, whereas inclusion of bulk solvent effects modifies the energy trend, making quite unfavorable the formation of the second DTBN−H_2O H-bond. This feature of the DTBN−water interaction is strongly system dependent; the high flexibility of the NO moiety and the steric repulsion of the two *tert*-butyl groups, evidenced by the large CNC angle value, actually decrease the portion of space around the NO moiety energetically accessible to water molecules. Again, a reliable description of solvent dynamics plays a crucial role in the accurate prediction of spectral observables.

(3) Short-range and dielectric effects of the solvent onto A_N and Δg_{iso}: the failure in describing the solvent dependence of nitrogen hyperfine coupling constant by a dielectric-based theory is due to the presence of strong specific solute−solvent interactions in the case of protic solvents. This means that a correct description of EPR solvent shifts should include both

short- and long-range effects, namely hydrogen bonding and electrostatic response. In the case of the DTBN−water system the discrete-continuum approach provides the chance of decoupling the different contributions and of quantifying their effect on each of the molecular parameters under investigation; the hydrogen bonding and the dielectric contributions, taken independently, have a roughly comparable effect for both A_N and Δg_{iso} values so that only their combined treatment leads to reliable results. The strength of the dielectric contribution decreases going from DTBN to DTBN−H_2O adducts. While the A_N value is reinforced, Δg_{iso} decreases going from gas phase to solution. After proper averaging over CPMD trajectories, the proposed discrete-continuum method provided solvent shifts in remarkable agreement with their experimental counterparts.

Of course, all these features of the nitroxide−water system are deeply interconnected, and the interplay of different structural, dynamical, and environmental effects calls for an effective computational approach, developed in an experiment-consistent fashion. As a matter of fact, the proposed "protocol" couples an effective treatment of electronic variables by state-of-the-art quantum chemistry calculations and the sampling of nuclear configurational space by first-principle atomistic simulations, thus providing not only a qualitative understanding of the underlying physicochemical processes but also a remarkable quantitative agreement of computed spectroscopic data with those obtained from experiments. The resulting integrated computational tool, consisting of sophisticated many-body methods, reliable HF-GGA hybrid density functionals, mixed discrete-continuum solvent models, and averaging from molecular dynamics simulations is becoming a valuable *in silico* complement to experimental results. Thanks to the implementation of all these items in user-friendly computer codes, this kind of analysis is or shortly will be feasible also by nonspecialists, and applied for much larger systems of biological and/or technological interest.

Acknowledgment. We thank Prof. O. Crescenzi (Naples) for valuable comments, the Italian Ministry for University and Research (MIUR) for financial support, and the Campus Grid at the University Federico II for computer facilities.

Supporting Information Available: Complete refs 11a, 11b, and 42. This material is available free of charge via the Internet at http://pubs.acs.org.

JA0574872